

Revisiting Mn-doped Ge using the Heyd-Scuseria-Ernzerhof hybrid functional

A. Stroppa,¹ G. Kresse,² and A. Continenza³¹CNR-SPIN L'Aquila, Italy²Faculty of Physics, and Center for Computational Materials Science, Universität Wien, Sensengasse 8/12, A-1090 Wien, Austria³CNISM-Dipartimento di Fisica Università degli Studi di L'Aquila, Via Vetoio 10 L'Aquila, Italy

(Received 30 June 2010; revised manuscript received 15 December 2010; published 9 February 2011)

We perform a comparative *ab initio* study of Mn-doped germanium semiconductor using the Perdew-Burke-Ernzerhof exchange-correlation functional, density functional theory (DFT) + U , and Heyd-Scuseria-Ernzerhof hybrid functional (HSE). We show that the HSE functional is able to correctly account for the relevant ground-state properties of the host matrix as well as of the Mn-doped semiconductor. Although the DFT + U and the HSE description are very similar, some differences still remain. In particular, the half metallicity is lost using DFT + U when a suitable U value, tuned to recover the photoemission spectra, is employed. For comparison, we also discuss the case of Mn in silicon.

DOI: 10.1103/PhysRevB.83.085201

PACS number(s): 71.15.Mb, 71.55.-i, 71.20.Nr, 71.23.An

I. INTRODUCTION

Dilute magnetic semiconductors (DMSs) are still a topic of great current interest.¹⁻⁴ The theoretical description of the interaction of transition-metal-doped semiconductors is challenging since localized states interact significantly with delocalized states. Density functional theory (DFT) in the local-density or generalized-gradient approximation (LDA or GGA) for the exchange-correlation energy is not able to properly describe the nonlocality of the screened exchange interaction and, furthermore, possesses a sizable self-interaction error.⁵ These limitations are particularly severe in the case of localized orbitals, for example, Mn-3*d* states, which are described as too shallow in energy, resulting in a large hybridization with anion *p* states. As a result, the Mn-3*d* states are over-delocalized. The situation is particularly serious in the case of small band-gap semiconductors (such as Ge) which are described as metals in LDA/GGA, thus producing an overestimated hybridization among the valence and conduction Ge states and Mn-*d* states. The physics of localized *d* states can be partially described using a DFT + U formalism, which introduces a local correction U to recover the proper position of the Mn-*d* states.⁶ However, in Ge, the accurate electronic properties are not completely recovered: for example, the half metallicity of the compound is lost within DFT + U scheme.

Very recently, hybrid Hartree-Fock density functionals, which mix a fraction of the exact Fock exchange with the DFT exchange, have been widely applied to extended solid-state systems.^{5,7-23} In this paper, we mainly focus on Mn-doping in bulk Ge by performing hybrid-DFT calculations. We show that the HSE functional gives a satisfactory description of the structural, electronic, and magnetic properties of Ge-based DMS, consistent with experimental data. Furthermore, for few selected properties, and, for the sake of comparison, we also include some results of Mn-doped silicon.

II. COMPUTATIONAL DETAILS

The calculations were performed within the projector augmented-wave (PAW) method²⁴ using the Perdew-Burke-Ernzerhof (PBE) GGA²⁵ and Heyd-Scuseria-Ernzerhof (HSE)

hybrid functional,^{26,27} recently implemented in the VASP code.^{28,29} We also used the DFT + U method for Mn within Dudarev's approach,³⁰ fixing U to 6 eV and J to 1 eV (PBE was used for the DFT part). The energy cutoff was set to 300 eV. Monkhorst-Pack *k*-point grids of $10 \times 10 \times 10$ and $6 \times 6 \times 6$ were used to sample the Brillouin zones of the Ge-bulk and the 64-atom unit cell, respectively. All the atomic internal positions were relaxed. In the following, we focus on the Ge bulk system, single (substitutional and interstitial) and double substitutional (dimer) Mn impurities in a 64-atom germanium cell. For silicon, we consider the bulk case and the Mn substitutional impurity in a 64-atom unit cell.

III. BULK GE

For bulk Ge, the calculated equilibrium properties are in good agreement with experiments: The HSE lattice constant is 5.703 (5.792) Å using HSE (PBE) within 0.7% (2.3%) of the experimental value of 5.660 Å;³¹ the HSE bulk modulus (731 kbar) improves over the PBE value (571 kbar) when compared to experiment (768 kbar³²). Furthermore, we remark that within HSE the energy gap is properly described to be indirect (0.63 eV including SOC³³ compared to the experimental value of 0.74 eV³⁴). A similar result was obtained within HSE for Si³³: the HSE lattice constant is 5.444 Å using HSE³³ compared to the experimental one of 5.430 Å.³² The calculated indirect energy gap is 1.12 eV,³³ while the experimental one is 1.17 eV.³² It is interesting to note that, for silicon, self-interaction schemes which are often used to improve the electronic structure description,^{5,35} do not open the gap.³⁶ This is important for our present study, since a faithful description of the equilibrium properties of the host semiconductor is at the basis of an appropriate description of the doped system.

IV. MN IMPURITIES IN GE

In Table I, we summarize our main results, that is, formation energy³⁷ (ΔH), Mn-Ge bond length ($d_{\text{Mn-Ge}}$) and the Mn magnetic moment (μ) at their respective theoretical lattice constants for the considered Mn-doping cases. The formation energies are evaluated with respect to the calculated Ge and Mn

TABLE I. Formation energy ΔH , Mn- X distances $d_{\text{Mn-}X}$ and magnetic moments μ for Mn-doped Ge for various structures. Distances in parentheses specify the ideal Ge-Ge bond-length of the host (lines $d_{\text{Mn-}X}$). Local Mn magnetic moment as well as total magnetic moment (in parentheses) are specified.

	PBE	DFT + U	HSE
Mn substitutional site			
ΔH (eV/Mn)	1.5		0.9
$d_{\text{Mn-Ge}}$ (Å)	2.46 (2.51)	2.53 (2.51)	2.52 (2.47)
μ (μ_B)	3.3 (3.1)	4.1 (3.4)	4.1 (3.0)
Mn interstitial site			
ΔH (eV/Mn)	2.1		1.8
$d_{\text{Mn-Ge}}$ (Å)	2.57 (2.51)	2.63 (2.51)	2.58 (2.47)
μ (μ_B)	3.4 (4.0)	4.2 (4.8)	3.8 (4.1)
Mn-Mn dimer			
ΔH_{AFM} (eV/Mn-pair)	2.9		1.5
$\Delta H_{\text{FM}} - \Delta H_{\text{AFM}}$	0.77	0.22	0.15
$d_{\text{Mn-Mn (FM)}}$ (Å)	2.55 (2.51)	2.97 (2.47)	2.99 (2.47)
$d_{\text{Mn-Mn (AFM)}}$ (Å)	1.95 (2.51)	2.71 (2.47)	2.83 (2.47)

equilibrium bulk phases [diamond Ge and antiferromagnetic (AFM)-fcc Mn]. Of course, while Ge-rich growth conditions can be safely assumed to fix the Ge chemical potential to its bulk value, the same is not true for Mn so that the formation energy is a function of the Mn chemical potential μ_{Mn} . In Table I we report the value for Mn-rich conditions fixing μ_{Mn} to the corresponding bulk value (α -Mn).

We note that the experimental evidence of *local* Ge-lattice dilation upon Mn-doping is correctly described using HSE yielding a Mn-Ge distance 2% larger than the ideal Ge-Ge bond length, while PBE gives a local contraction of -2% and DFT + U finds a smaller local dilation of 0.4% (0.8%) when using the theoretical PBE (HSE or experimental) lattice constant.^{38–40} The most recent extended x-ray absorption fine structure results^{41–43} yield a Mn-Ge coordination distance of $2.50\text{--}2.51 \pm 0.03$ Å for the samples obtained at low temperature and which are thought to be the best candidates for Mn occupation on substitutional sites.⁴² Clearly, these results match the HSE result and the DFT + U as well. Similar results for bond-length contraction/dilation within different DFT schemes were reported also for III–V-based DMSs.⁴⁴

A simple molecular orbital description, as sketched in Fig. 1, can be useful in order to describe the interaction of Mn in the tetrahedral Ge ligand field, as also done previously for similar compounds.⁴⁵ We recall that in diamondlike semiconductors, the sp valence states arrange to form sp^3 hybrid orbitals, each of them filled with a bonding electron pair. If one Ge atom is removed, creating a Ge vacancy, four sp^3 hybrids point toward the vacant Ge atom, each filled with one electron (dangling bonds). The Ge vacancy is now replaced by a Mn atom. Due to the local tetrahedral symmetry, the Mn d states are split into threefold degenerate t_{2g} and twofold degenerate e_g -like states, further split by the local exchange field (see Fig. 1, right part). From linear combinations of the four sp^3 Ge dangling bonds pointing toward the transition-metal impurity, an s -like $a_{1\uparrow,\downarrow}$ orbital and three p -like $t_{2g\uparrow,\downarrow}$ orbitals are formed. The host $a_{1\uparrow,\downarrow}$ orbital and the transition-metal $4s_{\uparrow,\downarrow}$ states form a doubly occupied

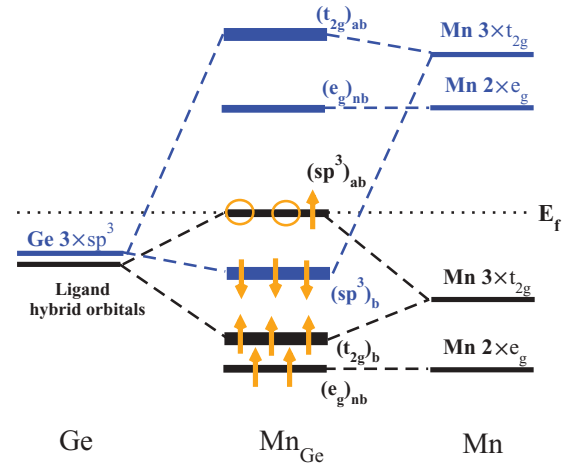


FIG. 1. (Color online) Molecular energy diagram of the Mn- d states (right) interacting with the Ge- sp^3 hybrid orbitals (left). The Mn- s states are not shown for clarity (see text). b , ab , and nb subscripts label bonding, antibonding, and nonbonding orbitals, respectively. Arrows denote up/down electrons while circles indicate holes. The central panel (Mn_{Ge}) shows p - d hybridization for substitutional Mn at Ge site.

bonding state deep in the semiconductor valence band, and an empty antibonding state high in the conduction band (not included in Fig. 1). For the majority component, the Mn- t_{2g} orbitals are lower in energy than the Ge- t_{2g} sp^3 hybrid states. They interact, giving rise to three bonding states ($3 \times \text{Mn-}t_{2g}$) $_b$ (see Fig. 1) and three antibonding states ($3 \times \text{Ge-}sp^3$) $_{ab}$. The Mn- e_g states do not hybridize because they are nonbonding in a tetrahedral ligand field. For the minority component, the Ge- t_{2g} sp^3 orbitals are lower in energy than the Mn- t_{2g} states. Upon interaction, they give rise to three bonding orbitals ($3 \times \text{Ge-}sp^3$) $_b$ and three antibonding orbitals ($3 \times \text{Mn-}t_{2g}$) $_{ab}$. The complex is characterized by a total of 11 electrons (4 from the nearest Ge atoms and 7 from the Mn impurity atom). Disregarding the 2 electrons occupying the lowest a_1 symmetrylike state, one needs to fill the orbitals with 9 electrons as shown in Fig. 1: Clearly, the Mn impurity is in a high spin state with 5 d electrons in the majority channel (2 electrons in the e_g and 3 in the t_{2g} -like states) and zero d electrons in the minority channels. However, while the minority valence Ge- sp^3 states are fully occupied, the majority states accommodate two holes. This simple molecular picture suggests that: (i) the compound is half metallic, with the Fermi level falling within the Ge majority valence band; (ii) the total spin moment of the complex, that is, $n_{\uparrow} - n_{\downarrow}$, is $3 \mu_B$; (iii) the local Mn d spin moment is $5 \mu_B$ partially compensated by the holes in the sp^3 states; (iv) the induced spin moment on the four nearest Ge atoms; that is, $n_{\uparrow}^{\text{Ge-}sp^3} - n_{\downarrow}^{\text{Ge-}sp^3}$ should be sizable and opposite to the spin on the Mn atom. In line with previous calculations,^{46–48} the calculated results (see Table I) confirm this picture finding a total spin moment of exactly $3 \mu_B$ in the unit cell, $4.1 \mu_B$ at the Mn atom, and $-0.11 \mu_B$ at the nearest Ge atoms. Furthermore, the sizable induced moments on Ge atoms suggest that the holes are rather delocalized.

The local angular momentum decomposed density of states (DOS) shown in Fig. 2 is consistent with this orbital interaction

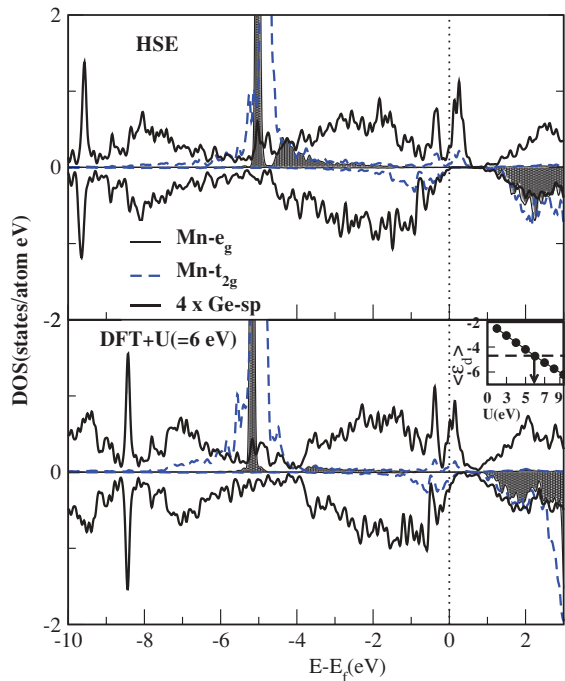


FIG. 2. (Color online) Density of states projected on the Mn impurity site (top) in symmetry-resolved angular momentum components: t_{2g} (dashed line) and e_g (shading) states for Mn substitutional impurity. The DOS projected on the $l = 1$ component of the 4 Ge (sp) coordinated with the Mn impurity is also shown (solid line). The inset shows the Mn- d center of mass as a function of the U value. The horizontal line indicates the value found within HSE.

diagram. The top panel shows the HSE results, whereas the bottom panel reports DFT + U results for $U = 6$ eV. In the inset, we show the relation between the center of mass of the Mn- d majority states, $\langle \epsilon_d \rangle$, and the U value. The horizontal line indicates the $\langle \epsilon_d \rangle$ value, which matches the HSE result ($U = 6$ eV). Figure 2 clearly confirms the interpretation discussed above. In particular, integration of the majority total DOS from the Fermi level up to the end of the Ge-valence band exactly sums up to two electrons: These are the two holes required to fill the Ge valence band. Mn substitution into the Ge host matrix does not produce a Jahn-Teller ion, but rather a Mn^{2+} ionic state with a d^5 configuration and two spin-polarized holes. Let us now compare the HSE and DFT + U DOS. Due to the choice of the U value, the Mn- d states have the same energy within HSE and DFT + U but the hybridization between Ge- sp and Mn t_{2g} and e_g states (this latter symmetry allowed away from Γ) is underestimated within DFT + U compared to HSE. While the on-site U mainly localizes the Mn d states, HSE also acts through the screened exchange on Ge- p states, lowering their energy position and leading to a larger Mn- d Ge- p hybridization. As a matter of fact, the larger hybridization in HSE compared to DFT + U can be recognized just below -4 eV, where a peak in the e_g character (shaded region in Fig. 2) is completely absent in the present DFT + U description. We note that previous LDA + U calculations⁶ with $U = 4$ eV, although reproducing the peak at -4 eV characteristic of the Mn-Ge bond,⁶ gave a quite different DOS for both the t_{2g} and the e_g states, which is due to the strong dependence of the localized d -states

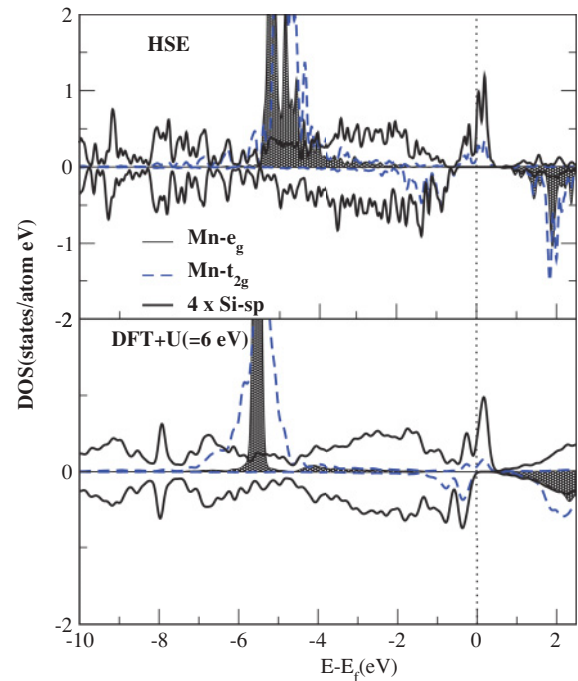


FIG. 3. (Color online) HSE DOS projected on the Mn impurity site (top) for Mn in Si. Labels as in Fig. 2. DFT + U , $U = 6$ eV (bottom).

description on the U parameter. Finally, as found in Ref. 6, the half-metallic character of the compound is destroyed within DFT + U : The energy position of the Mn- t_{2g} Ge- sp bonding minority states, whose energy position is mainly determined by the atomic Ge- sp levels, is raised toward higher energies causing an incomplete filling of the minority valence band.

In a previous study,⁴⁷ it was shown that the half metallicity is favored in Mn-doped Ge while in the silicon matrix it is lost. In Fig. 3, we show the HSE DOS for substitutional Mn_{Si} (top panel) and DFT + U , with $U = 6$ eV, the same used for Mn_{Ge} (bottom panel). The correction for the self-interaction error has a larger effect on Si- sp^3 states, since they are quite localized. Therefore, they are pushed down in energy. According to the orbital energy diagram shown in Fig. 1, also the minority bonding (Si- sp^3)_b are shifted down in energy, favoring the half metallicity. Obviously, the Mn- d states are also corrected for the self-interaction error, and they are pushed down in energy as well. On the other hand, DFT + U corrects only the Mn- d states, but not the Si- sp^3 states. This gives a near-half metallic structure and an underestimation of the hybridization of Mn-Si states compared to the HSE description.

A. The single interstitial impurity

This defect in a germanium matrix possesses twice the formation energy as the substitutional impurity (HSE); hence, it is unlikely to form. Here we only note that a tendency to a local expansion around Mn is found for all functionals. Interestingly, the local magnetic moment is larger for DFT + U than for HSE, suggesting sizable differences in the interaction of the impurity with the local environment.

B. Mn dimers

Double Mn substitutions on two nearest-neighbor Ge sites are of particular interest, since they are inferred to occur at experimental growth conditions^{41,48} leading to nucleation of Mn precipitates. In addition, they might be also detrimental for the magnetic ordering, since dimers show AFM coupling with no net spin moment. Unfortunately, GGA-based calculations are not entirely conclusive, since the dimer configuration becomes stable at a too-small bond length (1.95 Å) not compatible with the Mn ionic radius ($\simeq 1.1\text{--}1.3$ Å) or bond distances in Mn-Ge compounds. Thus, published results^{48,49} often refer to the ideal unrelaxed structure which, of course, strongly overestimates the heat of formation of the dimer. From the results reported in Table I, assuming thermodynamic equilibrium, we can comment on the relative concentration of single substitutional sites and dimers. At thermodynamic equilibrium, the concentration c of a defect with n_{Mn} Mn atoms is roughly proportional to $e^{-(\Delta H - n_{\text{Mn}}\Delta\mu_{\text{Mn}})/k_{\text{B}}T}$, where ΔH is the formation energy, k_{B} the Boltzmann constant, and T the temperature. Supposing $\Delta\mu_{\text{Mn}} \approx 0$ eV (thermodynamic equilibrium with α -Mn), the probability of finding a substitutional Mn or dimer is $e^{-0.9/k_{\text{B}}T}$ and $e^{-1.5/k_{\text{B}}T}$, respectively; that is, monomers are more likely to form than dimers. More generally, for a specific $\Delta\mu_{\text{Mn}}$ the probabilities for single substitutions and dimers are

$$e^{(-0.9 + \Delta\mu_{\text{Mn}})/k_{\text{B}}T} \quad \text{and} \quad e^{(-1.5 + 2\mu_{\Delta\text{Mn}})/k_{\text{B}}T}. \quad (1)$$

Therefore, the dimer concentration is larger than the monomer concentration only for $\Delta\mu_{\text{Mn}} > 0.6$ eV, that is at extremely Mn-rich conditions, where α -Mn precipitates are anyway already preferred over the formation of monomers (or dimers). Although kinetic effects might well hinder the nucleation of larger precipitates, our calculated thermodynamics suggests a rather low dimer concentration. It is important to note that the thermodynamic arguments alone, presented here, are not enough to fully discuss the relative probability of occurrence of the monomers with respects to dimers, as these systems are usually grown out of the thermodynamic equilibrium and kinetic effects may have an important role.

Finally, the stabilization energy of AFM over FM coupling of nearby impurities is much lower within HSE than GGA.

Furthermore, for HSE (and DFT + U), the calculated Mn-Mn distance for both FM and AFM magnetic alignment, are in line with experiments—always reporting local lattice dilation—as well as in line with the Mn-Mn distances in the FM Mn_5Ge_3 compound (varying between 2.52 and 3.06 Å).^{50–52}

V. CONCLUSIONS

In summary, we have performed a comparative study of substitutional Mn_{Ge} by using PBE, PBE + U , and HSE functional. The main focus is on the differences arising from three different treatments of the exchange-correlation term, namely, the PBE, DFT + U , and HSE. As is well known, the PBE treatment cannot describe satisfactorily the ground-state properties of the Mn in the host semiconductor matrix. Including the U correction at the DFT level improves the description. However, some differences still remain when compared to HSE. For example, the HSE Mn- d peak position is found at ~ -5 eV with respect to the Fermi energy, that is, in the same energy region as observed in photoemission experiments.⁶ When using the DFT + U method and fixing the U parameter in order to recover the experimental d -peak position, the hybridization with Ge- p states around -4 eV is underestimated compared to HSE and the experimental photoemission peak.⁶ Furthermore, for the same U , the half-metallic character is not predicted by DFT + U . The fact that HSE accurately describes the host semiconductor and, at the same time, the interaction of localized Mn states with the host valence states makes this functional a valuable approach for studying transition metal defects in semiconductors. It is also true that the HSE calculations are usually quite more computationally demanding with respect to DFT + U . Therefore, whenever a compromise between accuracy and computation effort is required in the calculations, a preliminary HSE study may be useful for choosing an appropriate U value, which is often not accessible from experiments.

ACKNOWLEDGMENTS

This work was supported by the Austrian Fonds zur Förderung der wissenschaftlichen Forschung and by a computing grant at the CINECA-HPC center.

¹T. Jungwirth, J. Sinova, J. Masek, J. Kucera, and A. MacDonald, *Rev. Mod. Phys.* **65**, 809 (2006).

²I. Zutic, J. Fabian, and S. D. Sarma, *Rev. Mod. Phys.* **76**, 323 (2004).

³T. Dietl, H. Ohno, F. Matsukura, J. Cibert, and D. Ferrand, *Science* **287**, 1019 (2000).

⁴E. Johnston-Halperin, J. A. Schuller, C. S. Gallinat, T. C. Kreutz, R. C. Myers, R. K. Kawakami, H. Knotz, A. C. Gossard, and D. D. Awschalom, *Phys. Rev. B* **68**, 165328 (2003).

⁵S. Kummel and L. Kronik, *Rev. Mod. Phys.* **80** (2008).

⁶L. Ottaviano, M. Passacantando, S. Picozzi, A. Continenza, R. Gunnella, A. Verna, G. Bihlmayer, G. Impellizzeri, and F. Priolo, *Appl. Phys. Lett.* **88**, 061907 (2006).

⁷A. Stroppa and G. Kresse, *Phys. Rev. B* **79**, 201201 (2009).

⁸M. Marsman, J. Paier, A. Stroppa, and G. Kresse, *J. Phys. Condens. Matter* **20**, 064201 (2008).

⁹F. Oba, A. Togo, I. Tanaka, J. Paier, and G. Kresse, *Phys. Rev. B* **77**, 245202 (2008).

¹⁰J. Paier, M. Marsman, K. Hummer, G. Kresse, I. C. Gerber, and J. Angyan, *J. Chem. Phys.* **124** (2006).

¹¹J. Paier, R. Hirschl, M. Marsman, and G. Kresse, *J. Chem. Phys.* **122**, 234102 (2005).

¹²D. Scanlon and G. Watson, *Chem. Mater.* **21**, 5435 (2009).

¹³D. O. Scanlon, B. J. Morgan, G. W. Watson, and A. Walsh, *Phys. Rev. Lett.* **103**, 096405 (2009).

¹⁴D. Scanlon, A. Walsh, and G. Watson, *Chem. Mater.* **21**, 4568 (2009).

¹⁵J. P. Allen, D. O. Scanlon, and G. W. Watson, *Phys. Rev. B* **81**, 161103(R) (2010).

¹⁶S. Lany and A. Zunger, *Phys. Rev. B* **81**, 205209 (2010).

- ¹⁷S. J. Clark, J. Robertson, S. Lany, and A. Zunger, *Phys. Rev. B* **81**, 115311 (2010).
- ¹⁸A. Janotti, J. B. Varley, P. Rinke, N. Umezawa, G. Kresse, and C. G. Van de Walle, *Phys. Rev. B* **81**, 085212 (2010).
- ¹⁹A. Stroppa and S. Picozzi, *Phys. Chem. Chem. Phys.* **12**, 5405 (2010).
- ²⁰A. Zunger, S. Lany, and H. Raebiger, *Physics* **3**, 53 (2010).
- ²¹C. Franchini, G. Kresse, and R. Podloucky, *Phys. Rev. Lett.* **102**, 256402 (2009).
- ²²C. Franchini, A. Sanna, M. Marsman, and G. Kresse, *Phys. Rev. B* **81**, 085213 (2010).
- ²³K. Hummer, J. Harl, and G. Kresse, *Phys. Rev. B* **80**, 115205 (2009).
- ²⁴P. E. Blöchl, *Phys. Rev. B* **50**, 17953 (1994).
- ²⁵J. P. Perdew, K. Burke, and M. Ernzerhof, *Phys. Rev. Lett.* **77**, 3865 (1996).
- ²⁶J. Heyd, G. E. Scuseria, and M. Ernzerhof, *J. Chem. Phys.* **118**, 8207 (2003).
- ²⁷J. Heyd, G. Scuseria, and M. Ernzerhof, *J. Chem. Phys.* **124**, 219906 (2006).
- ²⁸G. Kresse and J. Furthmüller, *Phys. Rev. B* **54**, 11169 (1996).
- ²⁹A. V. Krukau, O. A. Vydrov, A. F. Izmaylov, and G. E. Scuseria, *J. Chem. Phys.* **125**, 224106 (2006).
- ³⁰S. L. Dudarev, G. A. Botton, S. Y. Savrasov, C. J. Humphreys, and A. P. Sutton, *Phys. Rev. B* **57**, 1505 (1998).
- ³¹M. Fuchs, M. Bockstedte, E. Pehlke, and M. Scheffler, *Phys. Rev. B* **57**, 2134 (1998).
- ³²*Landolt-Bornstein: Numerical Data and Functional Relationships in Science and Technology*, edited by O. Madelung and M. Schulz (Springer-Verlag, Berlin, 1987), Vol. 22a, p. 251.
- ³³J. E. Peralta, J. Heyd, G. E. Scuseria, and R. L. Martin, *Phys. Rev. B* **74**, 073101 (2006).
- ³⁴O. Madelung, *Semiconductors: Data Handbook*, 3rd ed. (Springer, New York, 2004).
- ³⁵J. P. Perdew and A. Zunger, *Phys. Rev. B* **23**, 5048 (1981).
- ³⁶A. Filippetti and N. A. Spaldin, *Phys. Rev. B* **67**, 125109 (2003).
- ³⁷C. V. de Walle and J. Neugebauer, *J. Appl. Phys.* **95**, 3851 (2004).
- ³⁸S. Cho, S. Choi, S. C. Hong, Y. Kim, J. B. Ketterson, B.-J. Kim, Y. C. Kim, and J.-H. Jung, *Phys. Rev. B* **66**, 033303 (2002).
- ³⁹F. Tsui, L. He, A. Tkachuk, S. Vogt, and Y. S. Chu, *Phys. Rev. B* **69**, 081304 (2004).
- ⁴⁰F. Tsui, L. He, L. Ma, A. Tkachuk, Y. S. Chu, K. Nakajima, and T. Chikyow, *Phys. Rev. Lett.* **91**, 177203 (2003).
- ⁴¹L. Ottaviano, M. Passacantando, A. Verna, R. Gunnella, E. Principi, A. D. Cicco, G. Impellizzeri, and F. Priolo, *J. Appl. Phys.* **100**, 063528 (2006).
- ⁴²R. Gunnella, L. Morresi, N. Pinto, A. D. Cicco, L. Ottaviano, M. Passacantando, A. Verna, G. Impellizzeri, A. Irrera, and F. D'Acapito, *J. Phys. Condens. Matter* **22**, 216006 (2010).
- ⁴³M. Rovezzi, T. Devillers, E. Arras, F. d'Acapito, A. Barski, M. Jamet, and P. Pochet, *Appl. Phys. Lett.* **92**, 242510 (2008).
- ⁴⁴K. M. Yu, W. Walukiewicz, T. Wojtowics, I. Kuryliszyn, X. Liu, Y. Sasaki, and J. K. Furdyna, *Phys. Rev. B* **57**, 201303 (2002).
- ⁴⁵P. Mahadevan and A. Zunger, *Phys. Rev. B* **68**, 075202 (2003).
- ⁴⁶T. Schulthess and W. Butler, *J. Appl. Phys.* **89**, 7021 (2001).
- ⁴⁷A. Stroppa, S. Picozzi, A. Continenza, and A. J. Freeman, *Phys. Rev. B* **68**, 155203 (2003).
- ⁴⁸Y. D. Park, A. Y. Hanbicki, S. Erwin, C. Hellberg, J. Sullivan, J. Mattson, T. F. Ambrose, A. Wilson, G. Spanos, and B. Jonker, *Science* **295**, 651 (2002).
- ⁴⁹A. Continenza, G. Profeta, and S. Picozzi, *Appl. Phys. Lett.* **89**, 202510 (2006).
- ⁵⁰S. Picozzi, A. Continenza, and A. J. Freeman, *Phys. Rev. B* **70**, 235205 (2004).
- ⁵¹A. Stroppa, G. Kresse, and A. Continenza, *Appl. Phys. Lett.* **93**, 092502 (2008).
- ⁵²A. Stroppa and M. Peressi, *Phys. Status Solidi A* **204**, 44 (2007).